MATERIALS CHEMISTRY FRONTIERS

CCS 中国化学会 CHINESE CHEMICAL SOCIETY

ICCAS

ROYAL SOCIETY OF CHEMISTRY

RESEARCH ARTICLE

View Article Online
View Journal | View Issue

Check for updates

Cite this: *Mater. Chem. Front.*, 2021, **5**, 5328

Constructing a stable interface between the sulfide electrolyte and the Li metal anode *via* a Li^+-conductive gel polymer interlayer†

Ya-Hui Wang,[ab] Junpei Yue,[b] Wen-Peng Wang,[b] Wan-Ping Chen,[bc] Ying Zhang,[b] Yu-Guo Yang,[a] Juan Zhang,[bc] Ya-Xia Yin,[bc] Xing Zhang,*[bc] Sen Xin*[bc] and Yu-Guo Guo*[bc]

Due to high ionic conductivity, favorable mechanical plasticity, and non-flammable properties, inorganic sulfide solid electrolytes bring opportunities to the practical realization of rechargeable lithium–metal batteries with high energy, yet their use was impeded by an electrochemically unstable Li–electrolyte interface. Herein, we propose to address the issue *via* a Li^+-conductive gel polymer interlayer, which is derived *in situ* from a conventional liquid ether electrolyte during the cell fabrication process. The gel polymer interlayer not only enables intimate solid–solid contact and uniform Li-ion flux at the heterointerface but also effectively inhibits interfacial reactions and Li dendrite growth. With improved interfacial stability, a Li–Li symmetric cell with the gel polymer interlayer demonstrates an ultra-stable Li plating/stripping performance of over 1300 hours at 0.1 mA cm^{-2} and 350 hours at 0.5 mA cm^{-2} at room temperature, and a high critical current density of >5 mA cm^{-2}. This work offers general insights into a reasonable design of an anode/electrolyte interface for high-energy rechargeable Li–metal batteries.

Received 12th March 2021,
Accepted 5th May 2021

DOI: 10.1039/d1qm00395j

rsc.li/frontiers-materials

Published on 11 May 2021. Downloaded by Yunnan University on 8/23/2025 1:14:36 AM.

Introduction

Along with the rapid development of electric vehicles, distributed energy systems and smart electrical grids, batteries with high energy density and safety are in great demand.[1–6] In all battery technologies, all-solid-state batteries (ASSBs) based on solid-state electrolytes (SSEs) have been proposed to satisfy these requirements by combining lithium (Li) metals with high-voltage and chalcogen cathodes.[7–12] However, the unfavourable conductivity of SSEs and the large interfacial resistance between the Li anode and SSEs make it difficult to realize practical application for ASSBs.[13–17]

Lately, sulfide electrolytes (SEs) are being considered as one of the most promising solid electrolytes due to their excellent mechanical property (can be densified simply by cold pressing) and high ionic conductivity.[18,19] Among them, $Li_{10}GeP_2S_{12}$ (LGPS) with an ionic conductivity of 1.2×10^{-2} S cm^{-1} comparable with that of the liquid electrolytes and sufficient mechanical strength for resisting Li dendrite growth, exhibits the potential application in ASSBs.[20,21] Nevertheless, suffering from the poor compatibility between LGPS and the Li anode, the interfacial resistance could gradually increase and the Li dendrite could grow through the grain boundary or voids in SSEs, causing degradation of the battery performance.[14,22–28] In particular, LGPS will be reduced by metallic Li to form an electronic-ion mixed conductor interface (MCI) containing Li_2S, Li_3P, Li–Ge alloy, *etc.*, results in continuous interfacial parasitic reactions.[28–31] In the past few years, much effort has been devoted to improving the interfacial stability between SSEs and the Li anode by heteroatoms doping for LGPS, alloying of the Li metal and employing protective layers between SSEs and the Li anode.[32–38] Sun *et al.* reported a solid-state plastic crystal electrolyte (PCE) as an interlayer for a stable Li–LGPS interface.[39] Moreover, an inorganic Li_3N–LiF layer was employed by Wang *et al.* to achieve a dendrite-free solid-state electrolyte, where the highly ionic conductive Li_3N reduces the

[a] *School of Science, Beijing Jiaotong University, Beijing 100044, China*
[b] *CAS Key Laboratory of Molecular Nanostructure and Nanotechnology, CAS Research/Education Center for Excellence in Molecular Sciences, Beijing National Laboratory for Molecular Sciences (BNLMS), Institute of Chemistry, Chinese Academy of Sciences (CAS), Beijing 100190, China. E-mail: ygguo@iccas.ac.cn, xinsen08@iccas.ac.cn, zhangxing@iccas.ac.cn*
[c] *University of Chinese Academy of Sciences, Beijing 100049, China*

† Electronic supplementary information (ESI) available: Experimental section, materials characterization, electrochemical measurements, the specific values of resistances and the calculation result of ionic conductivity of Fig. 2b, Fig. S1b, detailed equivalent circuit of Fig. 2b and 4c, d, EIS spectrum of GPI-LGPS-GPI composite electrolytes, the EDS elemental mapping images of Li anode in Li|LGPS|Li system after 30 cycles, Li plating/stripping profiles of Li|LGPS|Li cells of 0.5 mA cm^{-2} for 0.5 mA h cm^{-2} at room temperature, F 1s, C 1s XPS spectrum of the cycled Li anode and LGPS pellet recovered from Li|GPI–LGPS–GPI|Li battery, and XPS binding energies with attributed species shown in Fig. 5 and Fig. S7, S8. See DOI: 10.1039/d1qm00395j

 This journal is © The Royal Society of Chemistry and the Chinese Chemical Society 2021

Published on 11 May 2021. Downloaded by Yunnan University on 8/23/2025 1:14:36 AM.

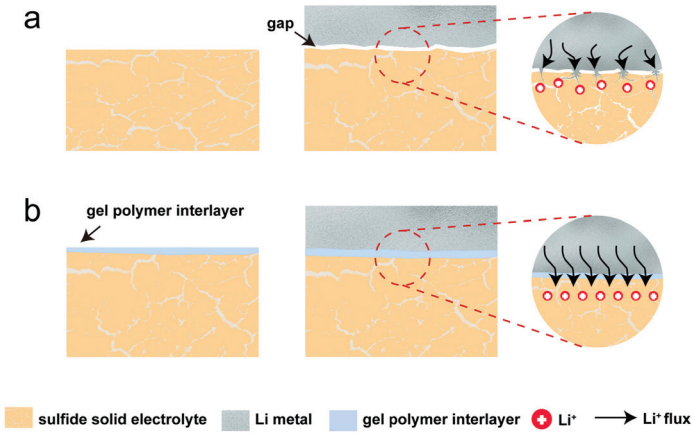

Fig. 1 Graphical illustration of the (a) unstable and (b) stable Li anode–SEs interface.

Li plating/stripping overpotential, and LiF with high interface energy plays a role in suppressing dendrites' growth.[40] Although many efforts have been carried out to stabilize the interface between the SSEs and the Li anode, building an *in situ* uniform and sustained protective layer between the interface of SSEs and the Li anode still remains challenging to achieve.

In this work, we demonstrated that a stable Li anode–SEs interface can be constructed through an *in situ* gelation strategy. An elastic gel polymer interlayer (GPI) was built to stabilize the interface of the Li anode and LGPS using *in situ* polymerization of 1,3-dioxolane (DOL) monomers with lithium hexafluorophosphate ($LiPF_6$) as an initiator.[41] Compared with the bare Li–SEs interface (Fig. 1a), the GPI introduced by *in situ* gelation strategy takes advantage of the beneficial properties of liquid precursors, ensuring good interfacial contact with interfaces, and then builds well-connected pathways that enable uniform Li^+ flux to restrain dendrite growth (Fig. 1b). The subsequent polymerization transforms the above liquid-state material to a quasi-solid material, which produces an elastic buffer layer to prevent side reaction at the interface. In addition, the low electronic conductivity of the GPI also facilitates dendrite suppression. Consequently, such *in situ* polymerized elastic GPI strategy provides a universal and facile method for steadying the Li–SEs interface and improving the cycling performance of Li metal batteries.

Result and discussion

First, the chemical compatibility between LGPS and solvents was investigated. Fig. 2a and Fig. S1a (ESI†) present the X-ray diffraction (XRD) patterns of LGPS powders immersed in different solvents. After immersing LGPS powder in DOL, 1,2-dimethoxyethane (DME) and DOL/DME (v:v, 1:1) mixed solvent for 24 hours, respectively, the characteristic peaks of the products are consistent with the pristine LGPS powder and no new peaks are generated, indicating good compatibility between LGPS and the above solvents. Furthermore, as shown

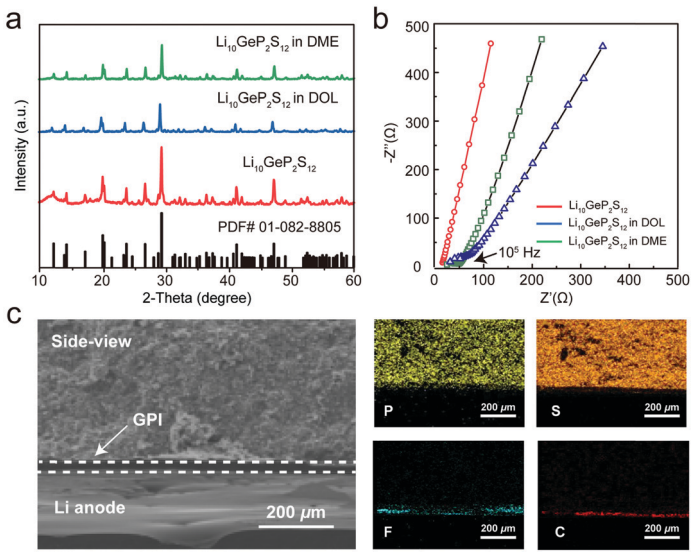

Fig. 2 (a) XRD pattern and (b) EIS spectrum of pristine LGPS, LGPS in DOL and DME after 24 hours, and (c) side-view SEM and EDS elemental mapping images of Li, GPI and LGPS.

Published on 11 May 2021. Downloaded by Yunnan University on 8/23/2025 1:14:36 AM.

in the electrochemical impedance spectrum (EIS) (Fig. 2b and Fig. S1b, ESI†), the high ionic conductivity (approx. 1.5 mS cm^{-1}) of the solvent-immersed LGPS is well-preserved compared with the pristine LGPS (Table S1 and Fig. S2, ESI†), in accord with ref.39. Such excellent stability together with the high ionic conductivity of LGPS was expected to exhibit great electrochemical performance towards efficient battery application. Subsequently, an elastic GPI was prepared by *in situ* polymerization of the precursor solution of 2 mol L^{-1} $LiPF_6$ and 1 mol L^{-1} bis(trifluoromethane) sulfonimide lithium salt (LiTFSI) into a DOL/DME (v:v, 1:1) mixed solvent. Meanwhile, the existence and morphology of GPI are investigated by scanning electron microscopy (SEM) and energy dispersive X-ray spectroscopy (EDS) elemental mapping. Fig. 2c shows the side view of the Li anode, GPI and LGPS after *in situ* polymerization. The thickness of the GPI is about 20 μm, and the EDS mapping confirms the elemental distribution S and P predominately located on the upper part of the cross-sectional view, while C and F are highly concentrated between Li and LGPS, suggesting that the GPI is covered uniformly on the surface of the Li anode. Moreover, it is imperative that the sandwich structure retains high ionic conductivity as shown in Fig. S3 (ESI†), implying the admirable electrochemical property of the structure.

Encouraged by the high ionic conductivity and stability of the sandwich structure, the symmetrical Li|LGPS|Li cell and the Li|GPI–LGPS–GPI|Li cell are assembled to investigate the interfacial stability of LGPS against the Li anode during cycling. First of all, the critical current density is examined at room temperature in symmetric Li|LGPS|Li and Li|GPI–LGPS–GPI|Li cells by gradually increasing currents from 0.1 to 5 mA cm^{-2} at the fixed capacity of 0.1 mA h cm^{-2}. As shown in Fig. 3a, the overpotential of Li|LGPS|Li increases significantly with the increase of current density, demonstrating that the interface of LGPS against the Li anode is unstable due to the serious interfacial reaction. Conversely, the overpotential of Li|GPI–LGPS–GPI|Li shows a finite increase with the increment of the current density.

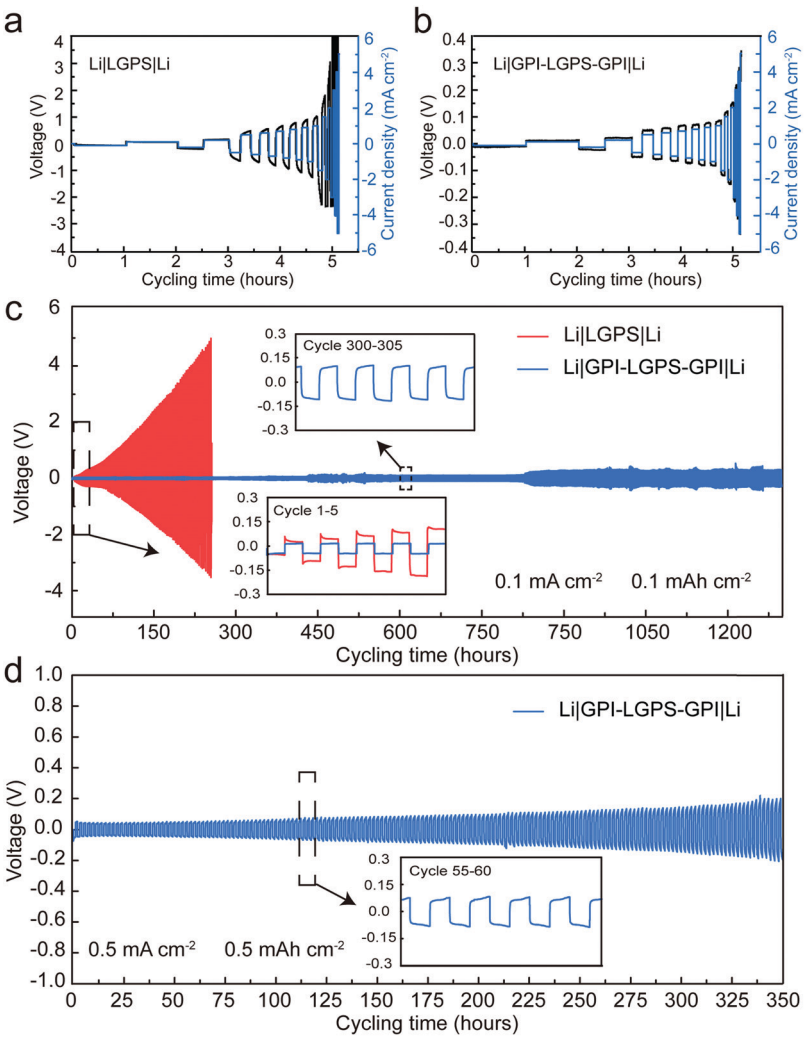

Fig. 3 Li plating/stripping overpotential profiles in the (a) Li|LGPS|Li cell and (b) Li|GPI–LGPS–GPI|Li cell at step-increased current densities. Comparison of the cycling stability of Li|LGPS|Li and Li|GPI–LGPS–GPI|Li symmetrical cells at room temperature with the current densities of (c) 0.1 mA cm^{-2} for 0.1 mA h cm^{-2} and (d) 0.5 mA cm^{-2} for 0.5 mA h cm^{-2}. Insets, detailed voltage profiles.

 This journal is © The Royal Society of Chemistry and the Chinese Chemical Society 2021

Published on 11 May 2021. Downloaded by Yunnan University on 8/23/2025 1:14:36 AM.

At 5 mA cm^{-2}, the overpotential of Li|LGPS|Li is over 4 V, while the overpotential of Li|GPI–LGPS–GPI|Li is only about 0.35 V, confirming that the introduction of GPI increases the critical current density and suppresses the parasitic reactions at the interface between the Li anode and LGPS (Fig. 3b). After that, we further performed a "Li strip/plate test" to estimate the dynamical interface stability and Li ion transport capability across the LGPS SE and Li metal interface. Fig. 3c compares the Li^+ plating/striping voltage profiles of the Li|LGPS|Li and Li|GPI–LGPS–GPI|Li cells within 1300 h at 0.1 mA cm^{-2} for 0.1 mA h cm^{-2}. In the first cycle, both cells showed a similar Li plating/stripping overpotential (approx. 40 mV). After 100 cycles, the overpotential of Li|LGPS|Li symmetric cells has exceeded 4 V, and the overpotential of Li|GPI–LGPS–GPI|Li cells remains at 40 mV. Meanwhile, the cell exhibits a flat and extraordinary stable plating/stripping profile even after prolonged 1300 h, indicating an increase in cycling stability because of the stable interface between LGPS and the Li anode. In addition, the Li|GPI–LGPS–GPI|Li symmetrical battery also exhibits a stable cycling for 350 h as the current density increases to 0.5 mA cm^{-2} (Fig. 3d), whereas the Li|LGPS|Li cell shows a considerable overpotential with prolonged time (Fig. S4, ESI†), further declaring the excellent Li plating/stripping of the GPI modified Li anode.

To better understand the interface stability and Li dendrite prevention ability of the GPI, the surface morphology of the Li anode after Li plating/stripping cycles is visually analysed using optical and SEM images, and the EIS of symmetric Li cells before and after cycles are also recorded. Fig. 4a and Fig. S5 (ESI†) show that substantial chunks composed of S, P, and Ge elements are generated on the surface of the pristine Li anode due to the serious parasitic reactions, while the GPI modified Li anode presents a smooth and flat surface (Fig. 4b), suggesting the successful protection from the GPI. These results are consistent with the performance of the Li symmetric batteries as shown in Fig. 3, namely, the introduction of the GPI layer significantly inhibits the side reaction of the Li–LGPS interface and depresses the growth of Li dendrites. Moreover, the electrochemical impedance spectroscopy (EIS) tests of Li symmetric cells before and after cycles exactly coincide with the earlier discussion. In accordance with the interfacial structure, the EIS could be considered as four distinct frequency regions, which correspond to the electrolyte bulk ($R_{SSE\text{-}b}$), grain boundary resistance ($R_{SSE\text{-}gb}$) and the interface resistance (R_{SUM}), and the electrochemical transfer polarization resistance of Li plating/stripping ($R_{LGPI\text{-}CT}$) (Fig. S6, ESI†).[33,42] Among them, the interphase resistance (R_{SUM}) could be subdivided into the Li–LGPS interphase resistance ($R_{Li\text{–}LGPS}$) or the combined effect of Li–GPI interphase resistance ($R_{Li\text{–}GPI}$) and GPI–LGPS interphase resistance ($R_{GPI\text{-}LGPS}$) for Li|LGPS|Li and Li|GPI–LGPS–GPI|Li cells, respectively. The interface of Li–LGPS during electrochemical operation continuously deteriorates due to the large volume variation and severe side reactions. The deteriorated interface with the enlarged surface area and poor ionic conductivity results in an increased interface resistance R_{SUM} with spreading frequency regions and the buried grain boundary resistance $R_{SSE\text{-}gb}$.[43,44] As shown in Fig. 4c, after 30 cycles, the R_{SUM} of the Li|LGPS|Li cell (70 kΩ) is greatly increased compared with that before cycle (Table S2, ESI†), indicating that a large number of poor ionic conductors were continuously produced on the Li–LGPS interface.[28,45,46] Conversely, the R_{SUM} of the modified Li|GPI–LGPS–GPI|Li cell remains unchanged after cycling (Table S2, ESI†), again demonstrating that the GPI as the interlayer between the Li metal and LGPS can block significant interfacial reactions between the Li metal and LGPS, thus promising a higher electrochemical stability (Fig. 4d). Furthermore, the unchanged $R_{SSE\text{-}b}$ and $R_{SSE\text{-}gb}$ at a high-frequency region (10^5 Hz) before and after cycles establish that there is no obvious decomposition of LGPS on the surface of the

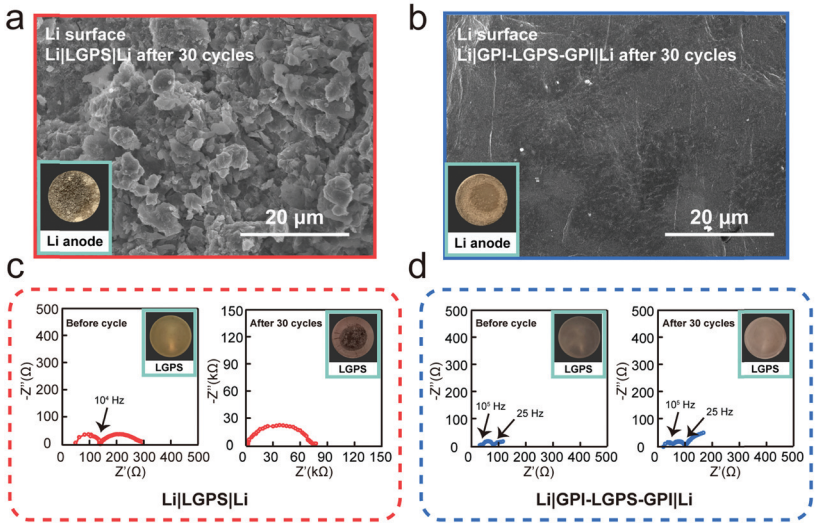

Fig. 4 SEM and optical images of the Li anode in the (a) Li|LGPS|Li and (b) Li|GPI–LGPS–GPI|Li system after 30 cycles, respectively. Nyquist plots and optical images of (c) Li|LGPS|Li and (d) Li|GPI–LGPS–GPI|Li cells before and after 30 cycles at the current density of 0.1 mA cm^{-2} for 0.1 mA h cm^{-2} accordingly.

Published on 11 May 2021. Downloaded by Yunnan University on 8/23/2025 1:14:36 AM.

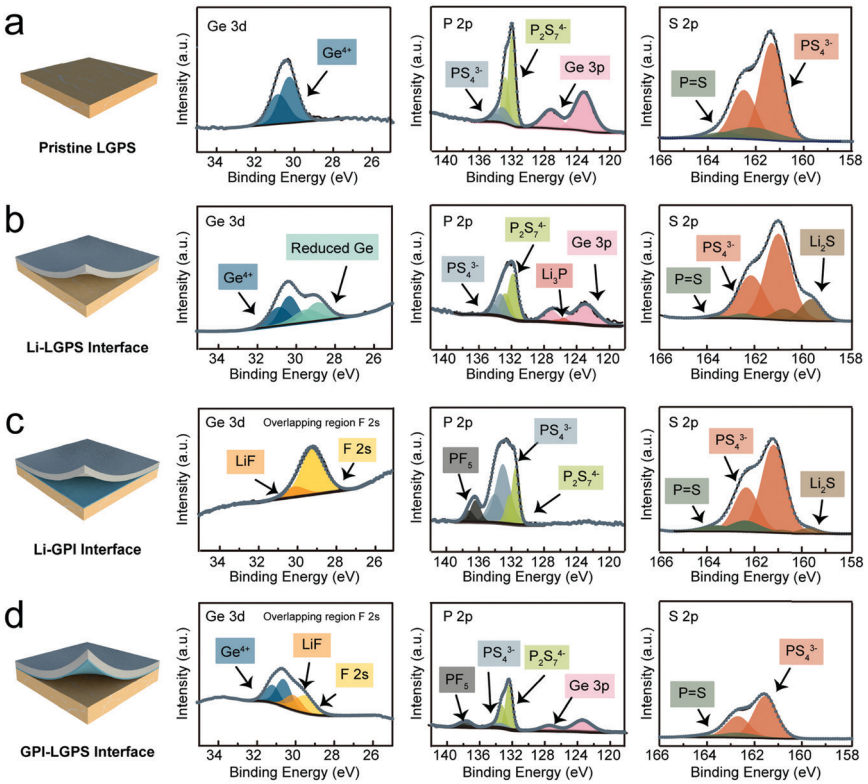

Fig. 5 Graphical illustrations and X-ray photoelectron spectroscopy (XPS) curves of the interfaces for (a) pristine LGPS, (b) Li–LGPS, (c) Li–GPI and (d) GPI–LGPS after 30 cycles at the current density of 0.1 mA cm^{-2} for 0.1 mA h cm^{-2} at room temperature.

Li|GPI–LGPS–GPI|Li cell (Fig. 4d and Table S2, ESI†), which is in accord with the above conclusion.[42]

In order to further explore an insight into the interphase structure change during Li plating/stripping, X-ray photoelectron spectroscopy (XPS) was used to characterize the composition and structure of Li–LGPS, Li–GPI and GPI–LGPS interfaces, respectively. As shown in Fig. 5a, no distinguishable peaks are observed for pure LGPS, which is consistent with the XRD result. Compared with pristine LGPS, Li_2S, Li_3P and reduced Ge components are detected on the LGPS–Li interface after cycling, where the peaks with binding energies of 159.66 (S $2p_{3/2}$), 125.28 (P $2p_{3/2}$) and 28.85 (Ge $3d_{5/2}$) eV in the XPS spectrum of the Li–LGPS interface can be assigned to Li_2S, Li_3P and reduced Ge, respectively (Fig. 5b and Table S3, ESI†).[37,39,40] Accordingly, Li|LGPS|Li exhibits poor Li plating/stripping performance because of the increasing interfacial resistance caused by poor ionic conductors of Li_2S and Li_3P components, consuming an electrolyte and deteriorating the interface continuously by reduced Ge.[31] Fig. 5c shows that there is no reduced Ge and Li_3P generated on the Li–GPI interface, while the peak at 30.3 (F 2s) and 159.66 (S $2p_{3/2}$) eV can be assigned to LiF and Li_2S, respectively (Fig. S7 and Table S4, ESI†), which could be derived from the decomposition of LiTFSI in the GPI, impressing that the GPI is chemically stable against the Li anode during cycling and is thus strong enough to protect the Li anode.[36,47] For the GPI–LGPS interface shown in Fig. 5d and Fig. S8 (ESI†), except for the presence of GPI components such as LiF and PF_5,[41] there is no significant change in the component and structure of cycled LGPS compared with pristine LGPS, indicating that a steady interface is constructed between the GPI and LGPS. The results exhibit that the as-obtained GPI layer could inhibit the decomposition of LGPS, suppress interfacial reactions and render a long lifespan of the Li metal anode and SEs.

Conclusions

In summary, we demonstrated an ingenious approach to construct an artificial elastic gel polymer interlayer (GPI) to stabilize the Li anode–SEs interface, where such a layer is *in situ* built *via* polymerization of DOL initiated by $LiPF_6$. The as-obtained GPI combines flexibility with stiffness, and enables sufficient solid–solid contact, avoiding current accumulation caused by point-to-point contact. Moreover, its high ionic conductivity and high Li^+ transference number (reported in our previous study) in combination with the mechanically stable interface uniform Li^+ flux at the interface. As a result, the Li|GPI–LGPS–GPI|Li symmetric cell demonstrates extra-stable Li plating/stripping over 1300 hours at 0.1 mA cm^{-2} and 350 hours at 0.5 mA cm^{-2} at room temperature. The present *in situ* gelation approach potentially provides a universal and efficient strategy to resolve the intrinsic interfacial issue toward the Li metal anode and SEs, and then paves the way for the next-generation high-energy solid-state Li metal batteries.

 This journal is © The Royal Society of Chemistry and the Chinese Chemical Society 2021

Published on 11 May 2021. Downloaded by Yunnan University on 8/23/2025 1:14:36 AM.

Author contributions

Ya-Hui Wang: conceptualization, methodology, investigation, data curation, visualization, writing – original draft, writing – review and editing. Jun-Pei Yue: conceptualization, writing – original draft, funding acquisition. Wen-Peng Wang: writing – original draft, visualization. Wan-Ping Chen: data curation, visualization. Ying Zhang: writing – review and editing. Yu-Guo Yang: writing – original draft, writing – review and editing. Juan Zhang: writing – review and editing. Ya-Xia Yin: writing – review and editing. Xing Zhang: conceptualization, writing – review and editing, supervision, project administration, funding acquisition. Sen Xin: conceptualization, writing – review and editing, supervision, project administration, funding acquisition. Yu-Guo Guo: conceptualization, writing – review and editing, supervision, project administration, funding acquisition.

Conflicts of interest

There are no conflicts of interest to declare.

Acknowledgements

This work was supported by the National Key R&D Program of China (Grant No. 2016YFA0202500 and 2019YFA0705700), the Basic Science Center Project of National Natural Science Foundation of China (Grant No. 51788104), the National Natural Science Foundation of China (Grant No. 21975266, 21773264, 21703257, 22005313 and 22005316), and the ''Transformational Technologies for Clean Energy and Demonstration,'' Strategic Priority Research Program of the Chinese Academy of Sciences under Grant No. XDA 21070300. S. X. acknowledges financial support from the start-up funds from the CAS. J. Yue acknowledges the China Postdoctoral Science Foundation Grant (No. 2019T120135). The authors thank Dr Z. J. Z., Dr X. Y. Z. and Dr Y. S. at the Center for Analysis and Testing, ICCAS for their help for the XPS and XRD analysis.

Notes and references

1 S. Chu and A. Majumdar, Opportunities and challenges for a sustainable energy future, *Nature*, 2012, **488**, 294–303.
2 Z. Y. Kou, Y. Lu, C. Miao, J. Q. Liu, C. J. Liu and W. Xiao, High-performance sandwiched hybrid solid electrolytes by coating polymer layers for all-solid-state lithium-ion batteries, *Rare Met.*, 2021, DOI: 10.1007/s12598-020-01678-w.
3 C. Z. Zhao, H. Duan, J. Q. Huang, J. Zhang, Q. Zhang, Y. G. Guo and L. J. Wan, Designing solid-state interfaces on lithium–metal anodes: A review, *Sci. China: Chem.*, 2019, **62**, 1286–1299.
4 Z. M. Zheng, H. H. Wu, H. D. Liu, Q. B. Zhang, X. He, S. C. Yu, V. Petrova, J. Feng, R. Kosteck, P. Liu, D. L. Peng, M. L. Liu and M. S. Wang, Achieving fast and durable lithium storage through amorphous FeP nanoparticles encapsulated in ultrathin 3D P-doped porous carbon nanosheets, *ACS Nano*, 2020, **14**, 9545–9561.
5 C. P. Yang, H. Xie, W. W. Ping, K. Fu, B. Y. Liu, J. C. Rao, J. Q. Dai, C. W. Wang, G. Pastel and L. B. Hu, An electron/ion dual-conductive alloy framework for high-rate and high-capacity solid-state lithium-metal batteries, *Adv. Mater.*, 2019, **31**, 1804815.
6 C. P. Yang, Y. G. Yao, S. M. He, H. Xie, E. Hitz and L. B. Hu, Ultrafine silver nanoparticles for seeded lithium deposition toward stable lithium metal anode, *Adv. Mater.*, 2017, **29**, 1702714.
7 Y. Zhang, T. T. Zuo, J. Popovic, K. Lim, Y. X. Yin, J. Maier and Y. G. Guo, Towards better Li metal anodes: Challenges and strategies, *Mater. Today*, 2020, **33**, 56–74.
8 J. R. He and A. Manthiram, 3D CoSe@C aerogel as a host for dendrite-free lithium–metal anode and efficient sulfur cathode in Li–S full cells, *Adv. Energy Mater.*, 2020, **10**, 2002654.
9 H. C. Gao, N. S. Grundish, Y. J. Zhao, A. J. Zhou and J. B. Goodenough, Formation of stable interphase of polymer-in-salt electrolyte in all-solid-state lithium batteries, *Energy Mater. Adv.*, 2021, 1932952.
10 W. P. Wang, J. Zhang, J. Chou, Y. X. Yin, Y. You, S. Xin and Y. G. Guo, Solidifying cathode–electrolyte interface for lithium–sulfur batteries, *Adv. Energy Mater.*, 2021, **11**, 2000791.
11 Z. Li and X. Guo, Integrated interface between composite electrolyte and cathode with low resistance enables ultra-long cycle-lifetime in solid-state lithium–metal batteries, *Sci. China: Chem.*, 2021, **64**, 673–680.
12 C. P. Yang, B. Y. Liu, F. Jiang, Y. Zhang, H. Xie, E. Hitz and L. B. Hu, Garnet/polymer hybrid ion-conducting protective layer for stable lithium metal anode, *Nano Res.*, 2017, **10**, 4256–4265.
13 Y. Y. Han, B. Liu, Z. Xiao, W. K. Zhang, X. L. Wang, G. X. Pan, Y. Xia, X. H. Xia and J. P. Tu, Interfaces issues of lithium metal anode for high energy batteries: Challenges, strategies, and perspectives, *InfoMat*, 2021, **3**, 155–174.
14 R. S. Chen, Q. H. Li, X. Q. Yu, L. Q. Chen and H. Li, Approaching practically accessible solid-state batteries: Stability issues related to solid electrolytes and interfaces, *Chem. Rev.*, 2019, **120**, 6820–6877.
15 Q. B. Zhang, Z. L. Gong and Y. Yang, Advance in interface and characterizations of sulfide solid electrolyte materials, *Acta Phys. Sin.*, 2020, **69**, 228803.
16 H. C. Wang, J. P. Zhu, Y. Su, Z. L. Gong and Y. Yong, Interfacial compatibility issues in rechargeable solid-state lithium metal batteries: A review, *Sci. China: Chem.*, 2021, DOI: 10.1007/s11426-021-9985-x.
17 C. P. Yang, K. Fu, Y. Zhang, E. Hitz and L. B. Hu, Protected lithium–metal anodes in batteries: From liquid to solid, *Adv. Mater.*, 2017, **29**, 1701169.
18 S. J. Chen, D. J. Xie, G. Z. Liu, J. P. Mwizerwa, Q. Zhang, Y. Zhao, X. X. Xu and X. Y. Yao, Sulfide solid electrolytes for all-solid-state lithium batteries: Structure, conductivity, stability and application, *Energy Storage Mater.*, 2018, **14**, 58–74.
19 A. Sakuda, A. Hayashi and M. Tatsumisago, Sulfide solid electrolyte with favorable mechanical property for all-solid-state lithium battery, *Sci. Rep.*, 2013, **3**, 1–5.

Published on 11 May 2021. Downloaded by Yunnan University on 8/23/2025 1:14:36 AM.

20 N. Kamaya, K. Homma, Y. Yamakawa, M. Hirayama, R. Kanno, M. Yonemura, T. Kamiyama, Y. Kato, S. Hama, K. Kawamoto and A. Mitusi, A lithium superionic conductor, *Nat. Mater.*, 2011, **10**, 682–686.

21 K. Kim, J. Park, G. Jeong, J. S. Yu, Y. C. Kim, M. S. Park, W. Cho and R. Kanno, Rational design of a composite electrode to realize a high-performance all-solid-state battery, *ChemSusChem*, 2019, **12**, 2637–2643.

22 Y. Z. Zhu, X. F. He and Y. F. Mo, Origin of outstanding stability in the lithium solid electrolyte materials: Insights from thermodynamic analyses based on first-principles calculations, *ACS Appl. Mater. Interfaces*, 2015, **7**, 23685–23693.

23 F. D. Han, Y. Z. Zhu, X. F. He, Y. F. Mo and C. S. Wang, Electrochemical stability of $Li_{10}GeP_2S_{12}$ and $Li_7La_3Zr_2O_{12}$ solid electrolytes, *Adv. Energy Mater.*, 2016, **6**, 1501590.

24 W. D. Richards, L. J. Miara, Y. Wang, J. C. Kim and G. Ceder, Interface stability in solid-state batteries, *Chem. Mater.*, 2016, **28**, 266–273.

25 M. Nagao, A. Hayashi, M. Tatsumisago, T. Kanetsuku, T. Tsuda and S. Kuwabata, In situ SEM study of a lithium deposition and dissolution mechanism in a bulk-type solid-state cell with a Li_2S–P_2S_5 solid electrolyte, *Phys. Chem. Chem. Phys.*, 2013, **15**, 18600–18606.

26 K. H. Park, Q. Bai, D. H. Kim, D. Y. Oh, Y. Z. Zhu, Y. F. Mo and Y. S. Jung, Design strategies, practical considerations, and new solution processes of sulfide solid electrolytes for all-solid-state batteries, *Adv. Energy Mater.*, 2018, **8**, 1800035.

27 Y. L. Sun, K. Suzuki, K. Hara, S. Hori, T.-a. Yano, M. Hara, M. Hirayama and R. Kanno, Oxygen substitution effects in $Li_{10}GeP_2S_{12}$ solid electrolyte, *J. Power Sources*, 2016, **324**, 798–803.

28 S. Wenzel, S. Randau, T. Leichtweiß, D. A. Weber, J. Sann, W. G. Zeier and J. Janek, Direct observation of the interfacial instability of the fast ionic conductor $Li_{10}GeP_2S_{12}$ at the lithium metal anode, *Chem. Mater.*, 2016, **28**, 2400–2407.

29 E. Umeshbabu, B. Z. Zheng, J. P. Zhu, H. C. Wang, Y. X. Li and Y. Yang, Stable cycling lithium–sulfur solid batteries with enhanced Li/$Li_{10}GeP_2S_{12}$ solid electrolyte interface stability, *ACS Appl. Mater. Interfaces*, 2019, **11**, 18436–18447.

30 Y. Z. Zhu, X. F. He and Y. F. Mo, First principles study on electrochemical and chemical stability of solid electrolyte–electrode interfaces in all-solid-state Li-ion batteries, *J. Mater. Chem. A*, 2016, **4**, 3253–3266.

31 P. Bron, B. Roling and S. Dehnen, Impedance characterization reveals mixed conducting interphases between sulfidic superionic conductors and lithium metal electrodes, *J. Power Sources*, 2017, **352**, 127–134.

32 T. Chen, L. Zhang, Z. X. Zhang, P. Li, H. Q. Wang, C. Yu, X. L. Yan, L. M. Wang and B. Xu, Argyrodite solid electrolyte with a stable interface and superior dendrite suppression capability realized by ZnO co-doping, *ACS Appl. Mater. Interfaces*, 2019, **11**, 40808–40816.

33 S. J. Choi, M. Jeon, W. D. Jung, S. Yang, S. Park, H. I. Ji, J. H. Lee, B. K. Kim, B. I. Sang and H. Kim, Robust solid-state interface with a deformable glass interlayer in sulfide-based all-solid-state batteries, *Solid State Ionics*, 2020, **346**, 115217.

34 F. D. Han, J. Yue, X. Y. Zhu and C. S. Wang, Suppressing Li dendrite formation in Li_2S–P_2S_5 solid electrolyte by LiI incorporation, *Adv. Energy Mater.*, 2018, **8**, 1703644.

35 Y. G. Lee, S. Fujiki, C. H. Jung, N. Suzuki, N. Yashiro, R. Omoda, D. S. Ko, T. Shiratsuchi, T. Sugimoto, S. Ryu, J. H. Ku, T. Watanabe, Y. S. Park, Y. Aihara, D. Im and I. T. Han, High-energy long-cycling all-solid-state lithium metal batteries enabled by silver–carbon composite anodes, *Nat. Energy*, 2020, **5**, 299–308.

36 J. W. Liang, X. N. Li, Y. Zhao, L. V. Goncharova, G. M. Wang, K. R. Adair, C. H. Wang, R. Y. Li, Y. C. Zhu, Y. T. Qian, L. Zhang, R. Yang, S. G. Lu and X. L. Sun, In situ Li_3P_{S4} solid-state electrolyte protection layers for superior long-life and high-rate lithium–metal anodes, *Adv. Mater.*, 2018, **30**, 1804684.

37 M. Q. Wang, Z. Peng, W. W. Luo, Q. Zhang, Z. D. Li, Y. Zhu, H. Lin, L. T. Cai, X. Y. Yao, C. Ouyang and D. Y. Wang, Improving the interfacial stability between lithium and solid-state electrolyte *via* dipole-structured lithium layer deposited on graphene oxide, *Adv. Sci.*, 2020, **7**, 2000237.

38 R. C. Xu, F. D. Han, X. Ji, X. L. Fan, J. P. Tu and C. S. Wang, Interface engineering of sulfide electrolytes for all-solid-state lithium batteries, *Nano Energy*, 2018, **53**, 958–966.

39 C. H. Wang, K. R. Adair, J. W. Liang, X. N. Li, Y. P. Sun, X. Li, J. W. Wang, Q. Sun, F. P. Zhao, X. T. Lin, R. Y. Li, H. Huang, L. Zhang, R. Yang, S. G. Lu and X. L. Sun, Solid-state plastic crystal electrolytes: Effective protection interlayers for sulfide-based all-solid-state lithium metal batteries, *Adv. Funct. Mater.*, 2019, **29**, 1900392.

40 X. Ji, S. Y. Hou, P. F. Wang, X. Z. He, N. Piao, J. Chen, X. L. Fan and C. S. Wang, Solid-state electrolyte design for lithium dendrite suppression, *Adv. Mater.*, 2020, **32**, 2002741.

41 F. Q. Liu, W. P. Wang, Y. X. Yin, S. F. Zhang, J. L. Shi, L. Wang, X. D. Zhang, Y. Zheng, J. J. Zhou, L. Li and Y. G. Guo, Upgrading traditional liquid electrolyte *via in situ* gelation for future lithium metal batteries, *Sci. Adv.*, 2018, **4**, eaat5383.

42 Y. Chen, W. W. Li, C. Z. Sun, J. Jin, Q. Wang, X. D. Chen, W. P. Zha and Z. Y. Wen, Sustained release-driven formation of ultrastable SEI between Li_6PS_5Cl and lithium anode for sulfide-based solid-state batteries, *Adv. Energy Mater.*, 2021, **11**, 2002545.

43 A. S. Westover, R. L. Sacci and N. Dudney, Electroanalytical measurement of interphase formation at a Li metal–solid electrolyte interface, *ACS Energy Lett.*, 2020, **5**, 3860–3867.

44 H. Xiao, L. B. Wu, Z. Huang, J. Lin and X. X. Xu, Characterization and testing of key electrical and electrochemical properties of lithium-ion solid electrolytes, *Energy Storage Sci. Technol.*, 2020, **9**, 479.

45 K. Takada, N. Ohta, L. Q. Zhang, X. X. Xu, B. T. Hang, T. Ohnishi, M. Osada and T. Sasaki, Interfacial phenomena in solid-state lithium battery with sulfide solid electrolyte, *Solid State Ionics*, 2012, **225**, 594–597.

 This journal is © The Royal Society of Chemistry and the Chinese Chemical Society 2021

46 J. Wan, Y. X. Song, W. P. Chen, H. J. Guo, Y. Shi, Y. J. Guo, J. L. Shi, Y. G. Guo, F. F. Jia and F. Y. Wang, Micromechanism in all-solid-state alloy-metal batteries: Regulating homogeneous lithium precipitation and flexible solid electrolyte interphase evolution, *J. Am. Chem. Soc.*, 2021, **143**(2), 839–848.

47 S. M. Xu, H. Duan, J. L. Shi, T. T. Zuo, X. C. Hu, S. Y. Lang, M. Yan, J. Y. Liang, Y. G. Yang, Q. H. Kong, X. Zhang and Y. G. Guo, *In situ* fluorinated solid electrolyte interphase towards long-life lithium metal anodes, *Nano Res.*, 2020, **13**, 430–436.

Published on 11 May 2021. Downloaded by Yunnan University on 8/23/2025 1:14:36 AM.